© 2018. Published by The Company of Biologists Ltd | Development (2018) 145, dev161976. doi:10.1242/dev.161976

RESEARCH ARTICLE

PDGF-A signaling is required for secondary alveolar septation and controls epithelial proliferation in the developing lung

Leonor Gouveia[1], Christer Betsholtz[1,2] and Johanna Andrae[1,*]

ABSTRACT

Platelet-derived growth factor A (PDGF-A) signaling through PDGF receptor α is essential for alveogenesis. Previous studies have shown that *Pdgfa*$^{-/-}$ mouse lungs have enlarged alveolar airspace with absence of secondary septation, both distinctive features of bronchopulmonary dysplasia. To study how PDGF-A signaling is involved in alveogenesis, we generated lung-specific *Pdgfa* knockout mice (*Pdgfa*$^{fl/-}$*; Spc-cre*) and characterized their phenotype postnatally. Histological differences between mutant mice and littermate controls were visible after the onset of alveogenesis and maintained until adulthood. Additionally, we generated *Pdgfa*$^{fl/-}$*; Spc-cre; Pdgfra*$^{GFP/+}$ mice in which *Pdgfra*$^{+}$ cells exhibit nuclear GFP expression. In the absence of PDGF-A, the number of *Pdgfra*$^{GFP+}$ cells was significantly decreased. In addition, proliferation of *Pdgfra*$^{GFP+}$ cells was reduced. During alveogenesis, *Pdgfra*$^{GFP+}$ myofibroblasts failed to form the α-smooth muscle actin rings necessary for alveolar secondary septation. These results indicate that PDGF-A signaling is involved in myofibroblast proliferation and migration. In addition, we show an increase in both the number and proliferation of alveolar type II cells in *Pdgfa*$^{fl/-}$*; Spc-cre* lungs, suggesting that the increased alveolar airspace is not caused solely by deficient myofibroblast function.

KEY WORDS: PDGF-A, PDGFRα, Alveogenesis, Lung development

INTRODUCTION

The presence of alveoli at the distal ends of the bronchial tree hugely increases the surface for gas exchange in the mammalian lung, and is a prerequisite for efficient breathing. Loss of alveolar structure leads to emphysema and chronic obstructive pulmonary dysplasia (COPD), which are disabling and life-threatening diseases. Alveolar structures comprise alveolar epithelial type 1 (AEC1) and type 2 (AEC2) cells in close contact with the capillary network, lined by mesenchymal cells such as lipofibroblasts and myofibroblasts (Beers and Morrisey, 2011; Chapman, 2011; Morrisey and Hogan, 2010; Warburton et al., 2010).

The process of alveolar maturation is known as alveogenesis. This final stage of lung development is initiated prenatally in humans, but postnatally in mice (McGowan, 2014; Shi et al., 2007; Warburton et al., 2010). The acinar buds at the end of the primitive bronchiolar saccules, which later give rise to the mature alveoli, are formed by thinning of the mesenchyme and continuing differentiation of both mesenchymal and epithelial cells during the sacculation stage of lung development (Treutlein et al., 2014; Warburton et al., 2010). At the end of this stage, lungs can support gas exchange but it is not efficient enough to fulfill the oxygen requirement (Pinkerton et al., 2014). To increase the surface area for gas exchange, the early postnatal alveolar structures are further divided by fishnet-like structures called septal ridges (Branchfield et al., 2016). The septal ridges restrict the ongoing epithelial expansion by creating secondary septae in the forming alveolar structures. This process is dependent on alpha smooth muscle actin (α-SMA) and elastin deposition from myofibroblasts surrounding the airways (Barron et al., 2016; McGowan, 2017; Moiseenko et al., 2017). Anomalous alveolar formation is a distinctive feature of bronchopulmonary dysplasia (BPD), a chronic illness usually observed in premature babies (Popova, 2013).

The platelet-derived growth factor (PDGF) family consists of four ligands (PDGF-A, -B, -C and -D) and two receptor tyrosine kinases (PDGFRα and β). They play important roles in development, homeostasis and disease, and downstream signaling from the PDGFRs is known to regulate cell differentiation, proliferation, migration, actin reorganization and apoptosis (reviewed by Andrae et al., 2008). In mice, PDGFRα and PDGF-A are expressed in the lung from embryonic time points to adulthood (Branchfield et al., 2016; Endale et al., 2017; Gouveia et al., 2017; Ntokou et al., 2015). Pioneering studies of global *Pdgfa* knockout (*Pdgfa*$^{-/-}$) mice demonstrated a role for PDGF-A in lung development. These *Pdgfa*-negative mice exhibited abnormally enlarged distal airspaces without signs of secondary septation, but because the mice died soon after birth a detailed analysis of lung morphology was not possible (Boström et al., 1996; Lindahl et al., 1997). The full *Pdgfra* knockout is early embryonic lethal (Soriano, 1997), but postnatally viable heterozygous mice combined with a hypomorphic *Pdgfa* allele also demonstrated dilated distal airspaces (Andrae et al., 2013). Other studies have shown that stromal cells obtained from premature infants with BPD have reduced levels of *Pdgfra* expression (Popova et al., 2014). Together, these observations suggest a role for PDGF-A signaling via PDGFRα in alveolar development.

Previous analyses of the *Pdgfa*$^{-/-}$ mice suggested several possible roles for PDGF-A in alveogenesis: (1) PDGFRα^{+} myofibroblast progenitors require PDGF-A to differentiate; (2) PDGF-A induces myofibroblast migration to the correct position in the alveolar niche; (3) myofibroblasts can migrate independently of PDGF-A but require it to execute their functions; (4) myofibroblast growth, proliferation and survival depend on PDGF-A (Boström et al., 1996). However, owing to the embryonic lethality of *Pdgfa*$^{-/-}$ mice it has not been possible to prove those hypotheses, even though they are often referred to as dogmas.

Here, we present a lung-specific *Pdgfa* knockout mouse (*Pdgfa*$^{fl/-}$*; Spc-cre*), which live into adulthood, thereby surpassing the early

[1]Department of Immunology, Genetics and Pathology, Rudbeck Laboratory, Uppsala University, SE-751 85 Uppsala, Sweden. [2]Integrated Cardio Metabolic Centre, Karolinska Institute, SE-141 57 Huddinge, Sweden.

*Author for correspondence (Johanna.andrae@igp.uu.se)

L.G., 0000-0002-3825-8571; C.B., 0000-0002-8494-971X; J.A., 0000-0003-0700-4381

Received 30 November 2017; Accepted 13 March 2018

Development (2018) 145, dev161976. doi:10.1242/dev.161976

lethality and putative systemic confounders of the global *Pdgfa* knockout mice. We show that deletion of PDGF-A in lung epithelial cells leads to impaired alveolar development resulting in enlarged alveoli lacking secondary septation. We suggest that PDGF-A signaling is required for the correct positioning and proliferation of myofibroblasts rather than their differentiation. In addition, as an indirect consequence of loss of the myofibroblast population, proliferation of AEC2s is increased, resulting in a higher number of AEC2s in mutant lungs.

RESULTS

Mice with a lung-specific deletion of *Pdgfa* survive into adulthood

In order to study the effect of *Pdgfa* deficiency on postnatal lung development in mice, it was necessary to circumvent the embryonic/perinatal lethality observed in $Pdgfa^{-/-}$ mice (Boström et al., 1996). We have previously shown that *Pdgfa* is expressed in airway epithelial cells and alveolar epithelial type-2 cells (AEC2s) in the lung (Gouveia et al., 2017), so we decided to use the Spc-cre mouse (Okubo and Hogan, 2004) to generate a lung-specific knockout mouse of *Pdgfa*. The breeding strategy (illustrated in Fig. 1A) generated four different genotypes: lung-specific *Pdgfa* knockout mice ($Pdgfa^{fl/-}$; *Spc-cre*), two variants of *Pdgfa* heterozygous mice ($Pdgfa^{fl/+}$; *Spc-cre* and $Pdgfa^{fl/-}$) and mice equivalent to *Pdgfa* wild-type mice ($Pdgfa^{fl/+}$). Initial analysis revealed a normal Mendelian distribution of the offspring genotypes (Fig. 1A) and no mutation-dependent lethality was observed. Mouse weight was followed until adulthood and no significant differences were observed between the different genotypes (Fig. 1B). Here, and in all further analyses of the $Pdgfa^{fl/-}$; *Spc-cre* mice, we used littermate $Pdgfa^{fl/+}$ mice as controls.

These results indicated that $Pdgfa^{fl/-}$; *Spc-cre* mice did not display the perinatal lethality observed in the $Pdgfa^{-/-}$ mice, and that they were a good model to study the role of PDGF-A during the development of the lung.

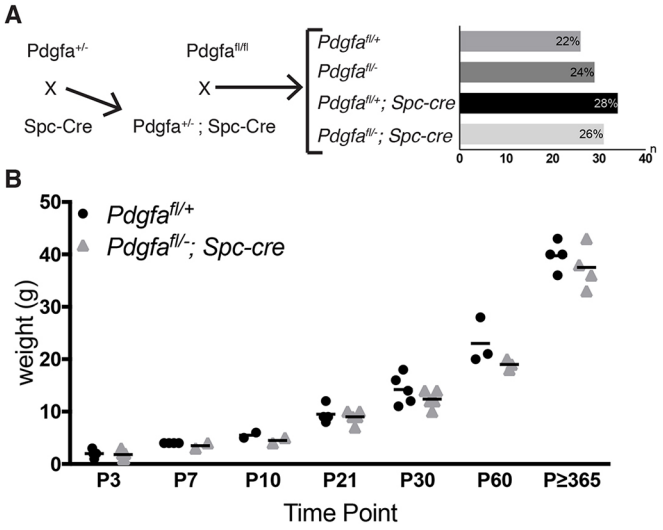

Fig. 1. Design of lung epithelial deletion of *Pdgfa*. (A) Breeding strategy to obtain $Pdgfa^{fl/-}$; *Spc-cre* mice. The graph shows the number (n) of individuals per genotype and the frequency (percentage) of the four offspring genotypes ($Pdgfa^{fl/+}$, $Pdgfa^{fl/-}$, $Pdgfa^{fl/+}$; *Spc-cre* and $Pdgfa^{fl/-}$; *Spc-cre*). (B) Growth curves for $Pdgfa^{fl/+}$ and $Pdgfa^{fl/-}$; *Spc-cre* mice displaying the weight in grams (*y*-axis) at different postnatal time points (*x*-axis). There was no statistical difference in weight at any time point ($P>0.05$; $n\geq4$ in each group).

Lung epithelial deletion of *Pdgfa* results in developmental arrest during alveogenesis

We compared the lungs of $Pdgfa^{fl/-}$; *Spc-cre* mice with $Pdgfa^{fl/+}$ mice before alveogenesis [postnatal day (P) 3], during alveogenesis (P7 and P10) and at the end of alveogenesis (P21). Quantitative PCR analysis of lung homogenates revealed an approximately 50% reduction in *Pdgfa* expression in $Pdgfa^{fl/-}$; *Spc-cre* lungs at each of the time points (Fig. 2A). These time points were also used for histological analysis of Hematoxylin and Eosin-stained lung sections, revealing morphological alterations in the lungs of $Pdgfa^{fl/-}$; *Spc-cre* mice. At P3, lungs of $Pdgfa^{fl/-}$; *Spc-cre* mice were histologically indistinguishable from littermate controls (Fig. 2B-D). Even though *Pdgfa* mRNA expression levels were significantly decreased at P3, neither the distal airspace area nor the

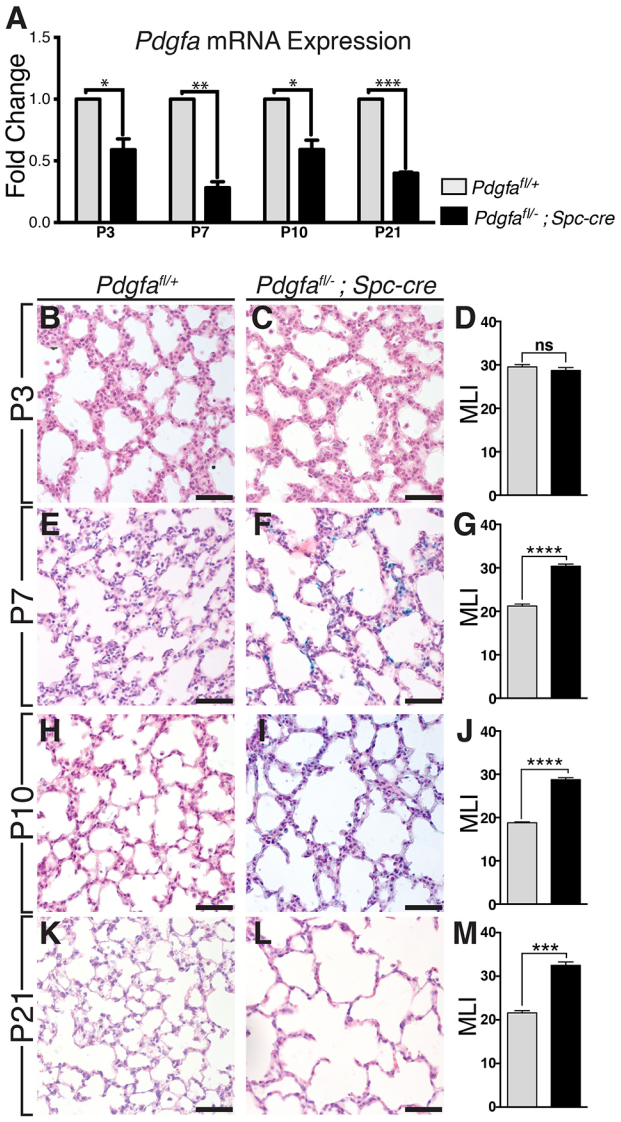

Fig. 2. Constitutive lung epithelial deletion of *Pdgfa* affects alveolar formation. (A) Quantitative PCR analysis of *Pdgfa* gene expression in control ($Pdgfa^{fl/+}$, $n=3$) and mutant ($Pdgfa^{fl/-}$; *Spc-cre*, $n=3$) lungs. (B-M) Morphological analysis of Hematoxylin and Eosin-stained $Pdgfa^{fl/+}$ (B,E,H,K) and $Pdgfa^{fl/-}$; *Spc-cre* (C,F,I,L) lungs verified with mean linear intercept (MLI) (D,G,J,M). Analyzed time points: P3 (B-D), P7 (E-G), P10 (H-J) and P21 (K-M). Graphs show mean+s.e.m. ns, non-significant; $^{*}P\leq0.05$, $^{**}P\leq0.01$, $^{***}P\leq0.001$, $^{****}P\leq0.0001$ (unpaired two-tailed *t*-test). Scale bars: 50 µm.

Development (2018) 145, dev161976. doi:10.1242/dev.161976

surrounding walls were phenotypically different from the control littermates. At P7, a significant increase of the alveolar airspace was detected in mutant lungs (Fig. 2E-G). At P10, mutant lungs failed to assemble alveoli correctly, demonstrated by a significant increase in the alveolar airspace in combination with a reduced number of forming alveolar septa (Fig. 2H-J). By P21, when alveolar formation was nearly completed, the mean linear intercept (MLI) of *Pdgfa*$^{fl/-}$; *Spc-cre* lungs was considerably increased with significant enlargement of the alveolar airspaces and fewer secondary septa compared with control lungs (Fig. 2K-M).

It was previously shown that *Pdgfa* signaling is not required for branching morphogenesis and that *Pdgfa*$^{-/-}$ lungs do not exhibit histological alterations before the onset of alveogenesis (Boström et al., 2002). However, it was unclear whether the observed phenotype in *Pdgfa*$^{-/-}$ lungs was an effect of an embryonic requirement for PDGF-A. To pinpoint the time point at which PDGF-A signaling is required, we used an inducible transgenic cre recombinase mouse (*Spc-cre*^{ERT2}) to knockout *Pdgfa* postnatally. Pups received tamoxifen from P0 for 5 days through the mother's milk and analysis was performed at P10 (Fig. 3A). The ability to induce *Pdgfa* deletion was confirmed with qPCR. The *Pdgfa*$^{fl/-}$; *Spc-cre*^{ERT2} knockout lungs exhibited a 50% decrease in *Pdgfa* mRNA expression levels (Fig. 3B), which was similar to that observed for *Pdgfa*$^{fl/-}$; *Spc-cre* mice (Fig. 2A). *Pdgfa*$^{fl/-}$; *Spc-cre*^{ERT2} lungs also presented a significant increase in the alveolar airspace (Fig. 3C) together with alveolar simplification compared with control lungs (Fig. 3D,E). These results indicate that postnatal deletion of *Pdgfa* is sufficient to mimic the lung phenotype seen when *Pdgfa* is deleted during embryonic lung development, and that the effects of *Pdgfa* deletion are important during secondary septation.

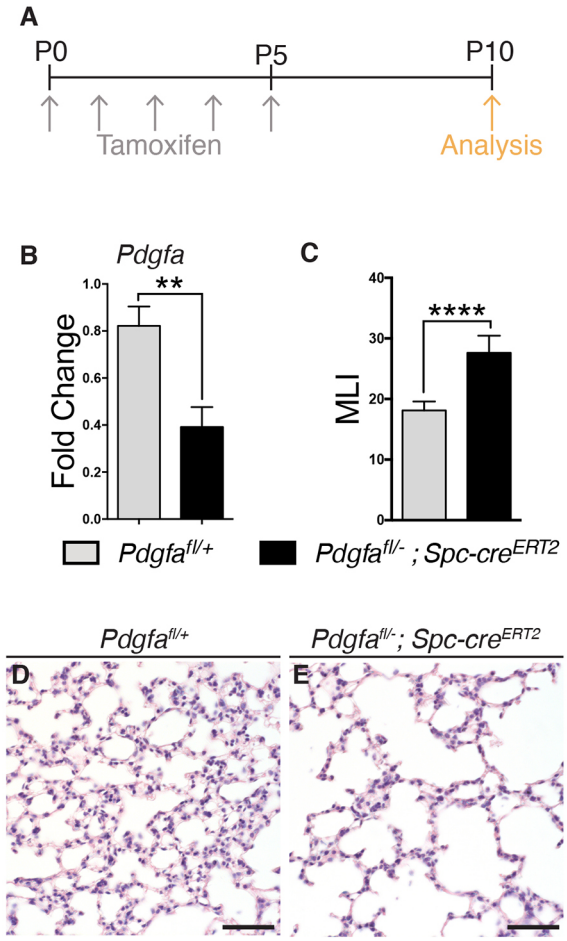

Fig. 3. Postnatal lung epithelial deletion of *Pdgfa* also affects alveolar formation. (A) Tamoxifen induction strategy. Pups received tamoxifen through the mother's milk every day from P0 to P5 and analysis of *Pdgfa*$^{fl/+}$ and *Pdgfa*$^{fl/-}$; *Spc-cre*^{ERT2} lungs was performed at P10. (B) Quantitative PCR of *Pdgfa* gene expression normalized to 18S rRNA; fold change is relative to control lungs (n=3 per group). (C) Comparison of mean linear intercept (MLI). (D,E) Hematoxylin and Eosin-stained lung sections from *Pdgfa*$^{fl/+}$ (D) and *Pdgfa*$^{fl/-}$; *Spc-cre*^{ERT2} (E) mice at P10. Graphs show mean+s.e.m. **P≤0.01, ****P≤0.0001 (unpaired two-tailed t-test, n=3 per group). Scale bars: 50 µm.

Pdgfra^{GFP} expression is decreased in *Pdgfa*$^{fl/-}$; *Spc-cre* lungs

To investigate whether epithelial deletion of *Pdgfa* affects the number of *Pdgfra*-positive cells, we combined *Pdgfa*$^{fl/-}$; *Spc-cre* mice with *Pdgfra*-GFP reporter mice. *Pdgfra*$^{H2B:GFP}$ mice carry an H2B:GFP fusion protein knocked into the *Pdgfra* gene, thus PDGFRα^{+} cells display nuclear GFP expression. *Pdgfra*$^{H2B:GFP}$ mice are also heterozygous null for *Pdgfra* (Hamilton et al., 2003).

We previously observed that the introduction of *Pdgfra*$^{GFP/+}$ worsened the lung phenotype in *Pdgfc*$^{-/-}$ mice (Andrae et al., 2016), and we therefore predicted a similar effect on the *Pdgfa*$^{fl/-}$; *Spc-cre* mice. However, we could not find any evidence for an aggravated lung phenotype in *Pdgfa*$^{fl/-}$; *Spc-cre*; *Pdgfra*$^{GFP/+}$ lungs compared with *Pdgfa*$^{fl/-}$; *Spc-cre* at P10. There was no significant difference in either lung morphology (Fig. 4A-D), nor in the mean linear intercept (Fig. 4E).

The effect on *Pdgfra* expression was examined by counting *Pdgfra*^{GFP}-positive cells in the alveolar region. Already at P3, *Pdgfa*$^{fl/-}$; *Spc-cre*; *Pdgfra*$^{GFP/+}$ lungs exhibited reduced GFP expression (Fig. 4F-I) and a significant decrease in the number of *Pdgfra*^{GFP}-positive cells (5.4±0.6%) compared with control lungs (16.4±1.3%) (Fig. 4J). During alveogenesis, there is normally an increase in *Pdgfra*$^{+}$ cells (Branchfield et al., 2016; Endale et al., 2017; Gouveia et al., 2017) in the alveolar region, reflecting a necessity for *Pdgfra*$^{+}$ cells during this stage of development. At P7, *Pdgfa*$^{fl/-}$; *Spc-cre*; *Pdgfra*$^{GFP/+}$ lungs sustained a significant decrease in the expression of *Pdgfra*^{GFP}-positive cells, compared with control lungs (Fig. 4L-O). The number of *Pdgfra*^{GFP}-positive cells per total number of cells was 25.9±3% in control lungs, whereas in the mutant lungs there were only 14.9±1.6% (Fig. 4P). The decreased *Pdgfra* expression at both time points was confirmed with qPCR (Fig. 4K,Q).

Pdgfa$^{fl/-}$; *Spc-cre* lungs fail to assemble α-smooth muscle actin rings properly during alveogenesis

We analyzed the expression of alpha smooth muscle actin (α-SMA) at P7. α-SMA expression in the alveolar region was detected in both control and knockout lungs, showing that even in the knockout conditions myofibroblasts were present (Fig. 5A-D). However, we observed striking differences between the patterns of expression. In control lungs, myofibroblasts showed high expression of *Pdgfra*-driven nuclear GFP, and these cells formed ring structures of α-SMA surrounding the forming alveoli, presumably creating the septal ridges responsible for alveolar septation (Fig. 5E,F). However, in *Pdgfa*$^{fl/-}$; *Spc-cre*; *Pdgfra*$^{GFP/+}$ lungs, expression of both nuclear GFP and α-SMA were markedly decreased (Fig. 5G,H). *Pdgfra* has previously been described as a marker also for lipofibroblasts in the mouse lung (Ntokou et al., 2015). To investigate the presence of lipofibroblasts in the mutant lungs, we stained for ADFP (perilipin 2). Expression of ADFP was lower in *Pdgfa*$^{fl/-}$; *Spc-cre*; *Pdgfra*$^{GFP/+}$ lungs than in the control lungs (Fig. 5I-L). These results indicate that the epithelial deletion of *Pdgfa*

Development (2018) 145, dev161976. doi:10.1242/dev.161976

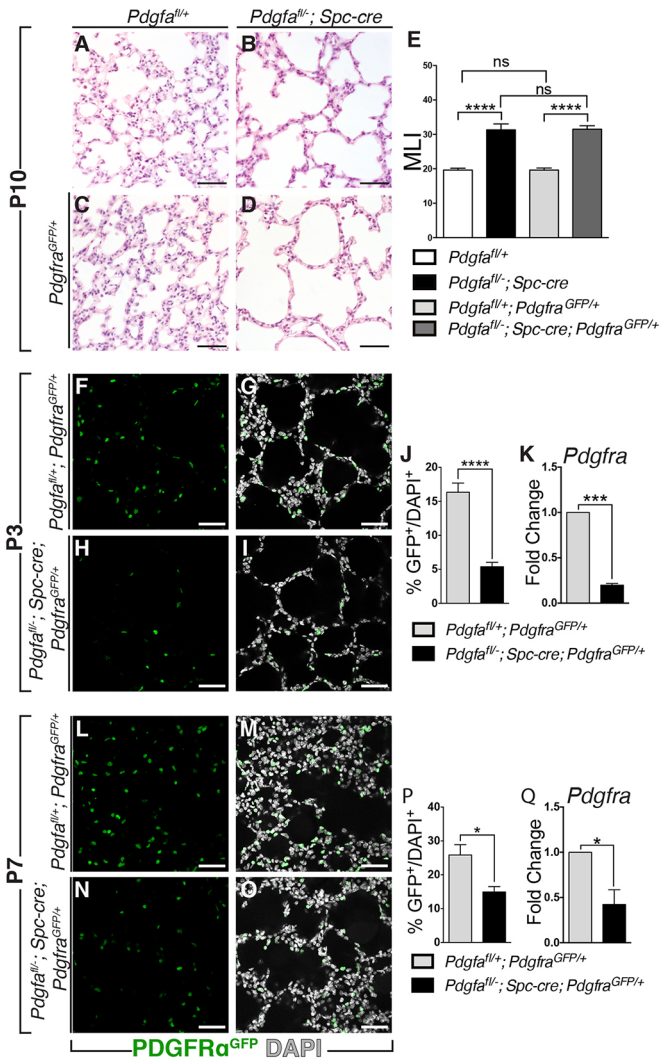

Fig. 4. *Pdgfa*$^{fl/-}$*; Spc-cre* lungs have reduced numbers of Pdgfra^{GFP}-positive cells. (A-D) Hematoxylin and Eosin-stained lung sections of control (A,C) and mutant (B,D) mice showing that heterozygosity of *Pdgfra* (by introduction of *Pdgfra*$^{GFP/+}$) did not worsen the lung morphology. (E) Mean linear intercept (MLI) quantification confirmed that there was no significant difference between *Pdgfa*$^{fl/+}$ and *Pdgfa*$^{fl/+}$*; Pdgfra*$^{GFP/+}$, and between *Pdgfa*$^{fl/-}$*; Spc-cre* and *Pdgfa*$^{fl/-}$*; Spc-cre; Pdgfra*$^{GFP/+}$. Differences between controls and mutants were still significant. (F-I) Cryosections of *Pdgfa*$^{fl/+}$*; Pdgfra*$^{GFP/+}$ (F,G) and *Pdgfa*$^{fl/-}$*; Spc-cre; Pdgfra*$^{GFP/+}$ (H,I) lungs at P3 showing *Pdgfra*^{GFP}-positive cells in green and DAPI in white. (J) Quantification of GFP-positive cells as a percentage of the total number of cells in control and mutant lungs at P3. (K) Quantitative PCR of *Pdgfra* gene expression in control and mutant lungs. (L-O) Cryosections of *Pdgfa*$^{fl/+}$*; Pdgfra*$^{GFP/+}$ (L,M) and *Pdgfa*$^{fl/-}$*; Spc-cre; Pdgfra*$^{GFP/+}$ (N,O) lungs at P7 showing *Pdgfra*^{GFP}-positive cells in green and DAPI in white. (P) Quantification of GFP-positive cells as a percentage of the total number of cells in control and mutant lungs at P7. (Q) Quantitative PCR of *Pdgfra* gene expression in control and mutant lungs. All graphs show mean+s.e.m. ns, non-significant; *P≤0.05, ***P≤0.001, ****P≤0.0001 (unpaired two-tailed *t*-test, n=3 per group). Scale bars: 50 µm.

most likely affected more than one population of *Pdgfra*$^{+}$ cells in the lungs.

To understand better the morphology of the α-SMA rings that surround the developing alveoli, we analyzed thick vibratome lung sections (100 µm) of mutant and control lungs. To our surprise, we found that α-SMA rings were present also in *Pdgfa*$^{fl/-}$*; Spc-cre; Pdgfra*$^{GFP/+}$ lungs (Fig. 6B,D), although this could not be appreciated in the thinner sections (Fig. 5C,D). At P3, both control and mutant lungs exhibited large α-SMA rings (≥50 µm in diameter) that surrounded the alveolar ducts with similar volume of actin per ring (Fig. 6A,B,I). The number and average diameter of the rings were different, however, with a significantly lower diameter in control lungs (65.8±2.7 µm) compared with mutant lungs (73.68±1.9 µm) (Fig. 6J). At P7, control lungs contained α-SMA rings with both low diameter (<50 µm) and large diameter (≥50 µm) surrounding the alveolar ducts (Fig. 6C,E,F,L). In contrast, mutant lungs never exhibited low diameter α-SMA rings (Fig. 6D,G,H,L). Moreover, in knockout lungs, the α-SMA rings were thinner and the volume of α-SMA per ring was significantly lower compared with the rings in control lungs (2403±162.5 µm^3 versus 3455±252.1 µm^3, respectively) (Fig. 6K).

The thick vibratome sections also enabled us to locate the *Pdgfra*$^{+}$ cells that formed the α-SMA rings. Fewer GFP^{+} cells formed the α-SMA rings in *Pdgfa*$^{fl/-}$*; Spc-cre; Pdgfra*$^{GFP/+}$ lungs (Fig. 6G,H) than in controls (Fig. 6E,F).

Interestingly, in *Pdgfa*$^{fl/-}$*; Spc-cre; Pdgfra*$^{GFP/+}$ lungs very few GFP^{+} cells were observed outside of the α-SMA rings (Fig. 6D), but such cells were more frequently observed in control lungs (Fig. 6C,F). This observation supports the hypothesis of a decrease in other *Pdgfra*$^{+}$ cell types, besides myofibroblasts.

Disruption of epithelial *Pdgfa* expression interferes with both mesenchymal and epithelial proliferation

Analysis of the cellular content of *Pdgfa*$^{fl/-}$*; Spc-cre* lungs at P3 revealed no difference in the number of cells per field image (Fig. S1A-C). However, at P7 *Pdgfa*$^{fl/-}$*; Spc-cre* lungs exhibited a significant reduction in the total number of cells per image field (Fig. S1D-F). The reduced number of cells in *Pdgfa*$^{fl/-}$*; Spc-cre* lungs was not a consequence of apoptosis, as there was no difference in expression of cleaved caspase 3 between control and *Pdgfa*$^{fl/-}$*; Spc-cre; Pdgfra*$^{GFP/+}$ lungs (data not shown). Proliferation was investigated by examining the expression of Ki67 (Mki67), but we could not detect any significant difference in the percentage of Ki67^{+} cells between control and *Pdgfa*$^{fl/-}$*; Spc-cre* lungs (12.85±1.3% and 12.72±1.9%, respectively; Fig. 7A,C,E,G,I). However, the number of *Pdgfra*$^{+}$/Ki67^{+} cells was significantly reduced in the *Pdgfa*$^{fl/-}$*; Spc-cre; Pdgfra*$^{GFP/+}$ lungs (Fig. 7B, arrowheads and 7D). Only 3.5±0.6% of *Pdgfra*$^{+}$ cells were also Ki67^{+} in the knockout lungs, compared with 7.1±0.9% in *Pdgfa*$^{fl/+}$*; Pdgfra*$^{GFP/+}$ lungs (Fig. 7J). These results indicate that *Pdgfra*$^{+}$ cells were less proliferative in *Pdgfa*$^{fl/-}$*; Spc-cre; Pdgfra*$^{GFP/+}$ lungs. Interestingly, we observed an increase in the relative number of Spc (Sftpc)$^{+}$ cells in knockout lungs at P7 (Fig. 7H,K). Moreover, proliferation of AEC2s (Spc^{+}/Ki67^{+}) in *Pdgfa*$^{fl/-}$*; Spc-cre; Pdgfra*$^{GFP/+}$ lungs was higher (13±3.1%) compared with controls (3.3±0.5%) (Fig. 7L) thus explaining why no decrease in overall proliferation was observed. AEC2s function as stem cells (Barkauskas et al., 2013) with the capacity of alveolar regeneration. It has been shown that EGFR/KRAS signaling can induce proliferation of AEC2s and is important for the self-renewal capacity of AEC2s (Desai et al., 2014). Quantitative PCR analysis revealed a significant increase in expression of the genes encoding the EGFR ligand HBEGF and KRAS in *Pdgfa*$^{fl/-}$*; Spc-cre; Pdgfra*$^{GFP/+}$ lung homogenates compared with control lungs (Fig. 7M,N), indicating activation of this pathway in the absence of *Pdgfa* signaling.

DISCUSSION

There is an increasing interest in deciphering the mechanisms of alveolar formation, motivated by the need to find therapies for diseases such as BPD and COPD. Recently, there have been several

Development (2018) 145, dev161976. doi:10.1242/dev.161976

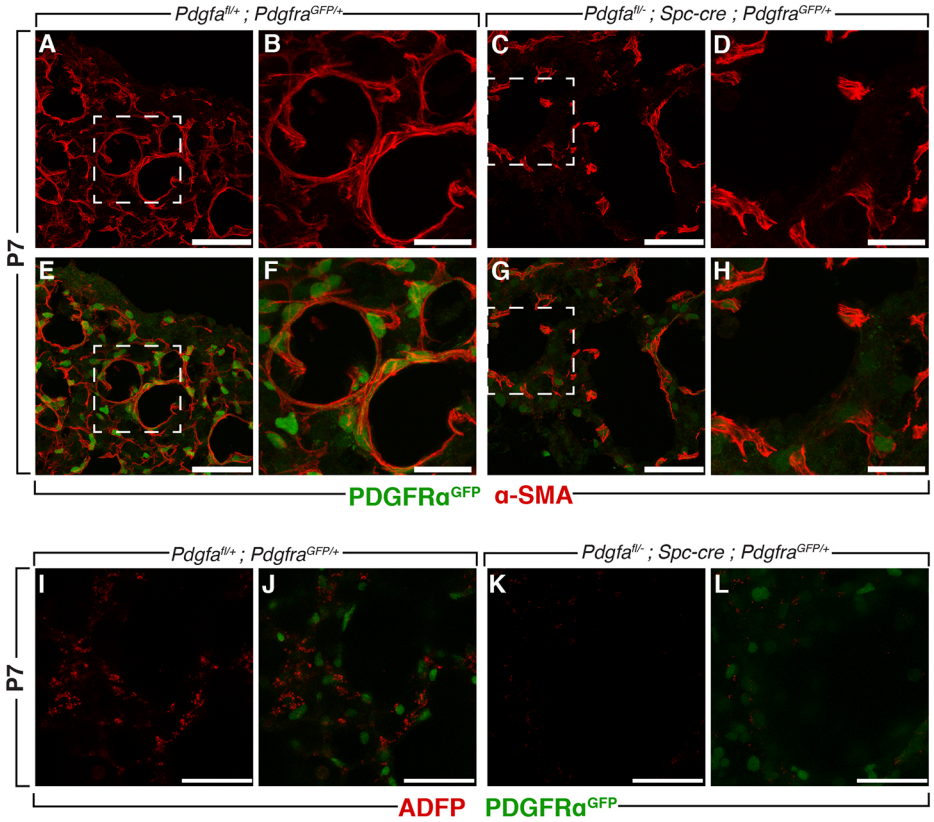

Fig. 5. Myofibroblasts and lipofibroblasts are dependent on *Pdgfa* expression in the lung. (A-H) Lung cryosections of *Pdgfa*$^{fl/+}$; *Pdgfra*$^{GFP/+}$ (A,B,E,F) and *Pdgfa*$^{fl/-}$; *Spc-cre*; *Pdgfra*$^{GFP/+}$ (C,D,G,H) lungs stained for α-SMA (red) and GFP (green, E-H) at P7. Areas within the white boxes in A,C,E,G are shown at high magnification in B,D,F,H, respectively. (I-L) Vibratome lung sections (100 µm) of *Pdgfa*$^{fl/+}$; *Pdgfra*$^{GFP/+}$ (I,J) and *Pdgfa*$^{fl/-}$; *Spc-cre*; *Pdgfra*$^{GFP/+}$ (K,L) at P7 showing GFP (green) and ADFP (red). Scale bars: 50 µm (A,C,E,G,I-L); 20 µm (B,D,F,H).

reports published describing PDGFRα expression in the lung (Branchfield et al., 2016; Endale et al., 2017; Gouveia et al., 2017; Green et al., 2016; Ntokou et al., 2015) highlighting the wish to understand better the role of PDGFRα signaling during lung development.

In this study, we created a new mouse model for studying the role of PDGF-A in the developing lung. By specifically deleting *Pdgfa* in the lung, we have been able to follow up on the seminal studies of *Pdgfa*$^{-/-}$ mice (Boström et al., 1996, 2002; Lindahl et al., 1997) by bypassing the perinatal lethality associated with the global knockout of *Pdgfa*. In addition, we obtained data that provide new information about the role of PDGFRα signaling in assembly of the actin cytoskeleton of myofibroblasts, as well as for mesenchymal-epithelial crosstalk during lung development.

The *Pdgfa*$^{fl/-}$*; Spc-cre* mice survived until adulthood, but they still exhibited the same lung phenotypes as observed in the *Pdgfa*$^{-/-}$ mice, suggesting that the lethality of the latter reflects other organ-specific or systemic effects of *Pdgfa*. Indeed, PDGF-A signaling has been implicated in developmental processes in many organs in addition to the lung, including the brain, gut, skin and testis (Fruttiger et al., 1999; Gnessi et al., 2000; Karlsson et al., 1999, 2000). Enlargement of the alveolar airspace and defective secondary septa formation were penetrant phenotypes in the *Pdgfa*$^{fl/-}$*; Spc-cre* mice even though *Spc-cre*-mediated deletion of *Pdgfa* only reduced the total expression of *Pdgfa* to approximately 50%. This reveals the importance of PDGF-A expression by *Spc*$^{+}$ cells for alveolar formation. The remaining 50% *Pdgfa* expression could be attributed to expression in the proximal lung airway epithelia and smooth muscle cells, as previously described (Gouveia et al., 2017).

The observed phenotype was not a consequence of embryonic effects of *Pdgfa* deletion. We observed the same phenotype when inducing the deletion at birth as when deleting *Pdgfa* in the embryo. Moreover, mutant lungs were histologically indistinguishable from controls at P3, supporting our hypothesis that PDGF-A signaling is important mainly during the alveolar stage. Nevertheless, we observed a lower number of *Pdgfra*$^{+}$ cells at P3, combined with a larger diameter of the α-SMA rings surrounding the forming alveolar structures. As these observations did not result in evident deficiency in the primary septa or duct formation, we believe that signaling pathways other than PDGF-A/PDGFRα are more important for the developmental processes preceding alveogenesis. For example, Notch inactivation in the distal epithelium causes enlargement of the alveolar structures combined with a decrease in proliferative *Spc*$^{+}$ cells at P3 (Tsao et al., 2016), which we did not observe in our model.

We show in our model that *Pdgfra* expression decreased upon lung-specific deletion of *Pdgfa*, which seemed to affect different populations of *Pdgfra*$^{+}$ cells such as myofibroblasts and lipofibroblasts. Our observations indicate that myofibroblasts are indeed capable of differentiating in *Pdgfa*$^{fl/-}$*; Spc-cre* lungs, as α-SMA expression was detected in the alveolar region at P7. The small α-SMA^{+} rings formed by *Pdgfra*$^{+}$ myofibroblasts in control lungs had a diameter that fits with the forming septal ridges. These α-SMA^{+} rings were formed by multiple myofibroblasts similar to the multicellular contractile structures described in the healing of epithelial wounds. During the wound closure process, the cells at the border of a wound form one thick actin ring that contracts, thereby bringing the edges of the wound together (Tamada et al., 2007; Vedula et al., 2015). In a similar way, the small α-SMA^{+} rings formed by multiple myofibroblasts surrounding the alveoli contract and create a tension that restricts alveolar expansion, thus creating the septal ridges. The lack of formation of small α-SMA^{+} rings in *Pdgfa*$^{fl/-}$*; Spc-cre* lungs reflects the reduced ability of the myofibroblasts to surround the alveoli, contract and create the septal ridges in the correct manner. In the absence of contraction, the alveoli

Development (2018) 145, dev161976. doi:10.1242/dev.161976

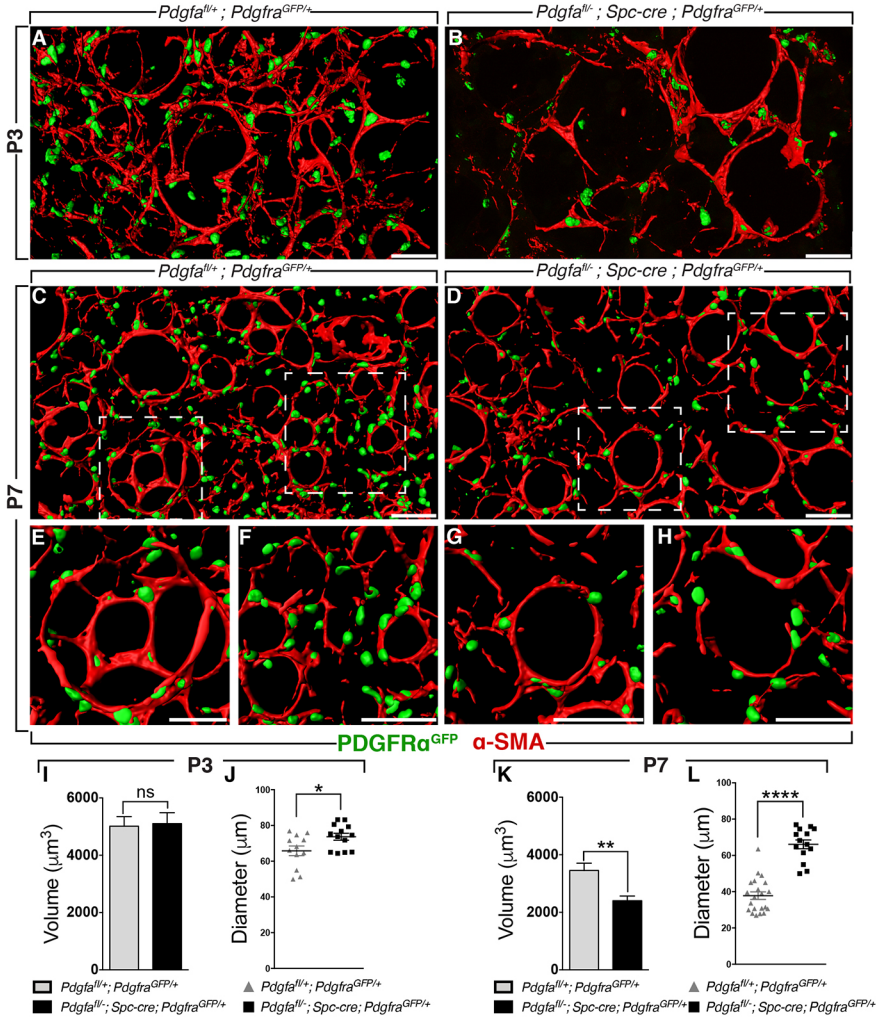

Fig. 6. Defective alveolar α-SMA ring formation in *Pdgfa*$^{fl-}$*; Spc-cre* lungs. (A-H) 3D projection images of thick lung vibratome sections (100 µm) showing the volume of α-SMA rings (red) and *Pdgfra*^{GFP}-positive nuclei (green), at P3 (A,B) and P7 (C-H). E-H show high-magnification images of the regions marked with white boxes in C and D, respectively. (I) Volume of individual α-SMA rings at P3 in control and mutant lungs. (J) Diameter of individual rings at P3 in control and mutant lungs. (K) Volume of individual α-SMA rings at P7 in control and mutant lungs. (L) Diameter of individual rings at P7 in control and mutant lungs. All graphs show mean±s.e.m. ns, non-significant; *P≤0.05, **P≤0.01, ****P≤0.0001 (unpaired two-tailed *t*-test, n=3 per group). Scale bars: 50 µm.

are unrestrained and free to expand and create the observed enlarged alveolar airspaces.

The mechanisms that trigger *Pdgfra*$^+$ myofibroblasts to express α-SMA and form the contractile rings are still unclear. It is known that inhalation and exhalation cause mechanical stretch in the lung (Roan and Waters, 2011). Recently, it was proposed that fibroblast mechanosensitivity *in vitro* depends on *Pdgfra* expression (McGowan and McCoy, 2017). A likely hypothesis is therefore that respiration after birth induces mechanical stretch, which triggers *Pdgfra*$^+$ myofibroblasts to migrate, spread around the developing alveoli and form multicellular rings of α-SMA. In our model (in the absence of PDGF-A signaling from AEC2s), *Pdgfra* was downregulated in myofibroblasts, which became less responsive to mechanical stretch and failed to occupy their correct position and create the necessary small α-SMA rings.

Pdgfra$^+$ fibroblasts produce extracellular matrix proteins and analyses of gene expression revealed changes in, for example, *Col1a1* and *Eln* in the *Pdgfa*$^{fl/-}$*; Spc-cre* mice (data not shown). This is being followed up in an upcoming project with a focus on adult mice and their response to injury.

We propose that the enlargement of the alveolar airspace in *Pdgfa*$^{fl/-}$*; Spc-cre* lungs is caused by unresponsive myofibroblasts in combination with deregulated AEC2 proliferation. In a recent study, a population of *Pdgfra*$^+$ cells (named mesenchymal alveolar niche cells or MANCs) identified in close proximity to AEC2s played a role in alveolar epithelial self-renewal (Zepp et al., 2017). The authors identified several signaling pathways (with ligands expressed by MANCs and receptors expressed by AEC2s) supporting the crosstalk between these two cell types. We suggest that the deletion of *Pdgfa* affects this crosstalk and results in an indirect effect on the proliferation of *Spc*$^+$ cells.

The increased proliferation of AEC2s together with the increased gene expression of EGFR ligand in *Pdgfa*$^{fl/-}$*; Spc-cre* mutant lungs point to a role for PDGF-A in the stem cell function of AEC2s. It has been shown that *Pdgfra*$^+$ fibroblasts accelerate the conversion of AEC2s to AEC1s *in vitro* (Barkauskas et al., 2013). Additionally, Desai and colleagues showed that only a small fraction of AEC2s have the capacity to both self-renew and convert to AEC1s. The authors hypothesized that a dominant AEC2 stem cell prevents neighboring AEC2s from being activated and participating in the renewal of AECs (Desai et al., 2014). We further hypothesize that PDGF-A is involved in that neighboring cell suppression, as deletion of *Pdgfa* expression in *Spc*$^+$ cells resulted in an increased number of AEC2s and altered proliferation. Further studies will be necessary regarding the stem cell capacity of *Pdgfa*$^+$ AEC2s.

MATERIALS AND METHODS

Ethical statement

All experiments were approved by the Uppsala animal ethics committee (permit number C224/12 and C115/15) and performed according to Swedish legislation.

Development (2018) 145, dev161976. doi:10.1242/dev.161976

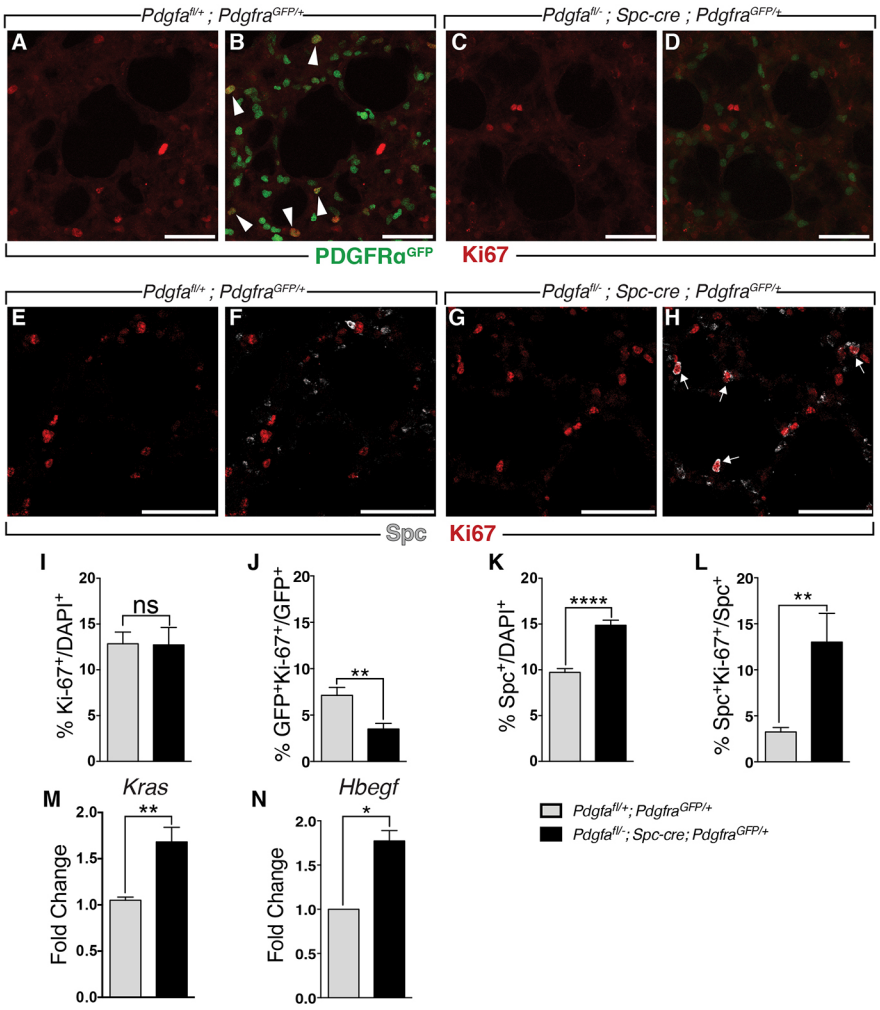

Fig. 7. Differences in proliferation between control and mutant lungs. (A-D) Vibratome P7 lung sections (100 µm) showing *Pdgfra*^{GFP}-positive cells (green) and proliferating Ki67-positive cells (red) in control (A,B) and mutant (C,D) lungs. Arrowheads in B indicate GFP$^+$/Ki67$^+$ cells. (E-H) Paraffin P7 lung sections (5 µm) stained for Spc (gray) and Ki67 (red) in control (E,F) and mutant (G,H) lungs. Arrows in H indicate Spc$^+$/Ki67$^+$ cells. (I-L) Quantification data comparing control (n=3) and mutant lungs (n=3): (I) proliferating cells (Ki67$^+$) as a percentage of total number of cells, (J) proliferating GFP-positive cells (GFP$^+$/Ki67$^+$) as a percentage of total number of GFP-positive cells, (K) AE2 cells (Spc$^+$) as a percentage of total number of cells, (L) proliferating AE2 cells (Spc$^+$/Ki67$^+$) as a percentage of Spc-positive cells. Quantitative PCR of *Kras* (M) and *Hbegf* (N) gene expression in control (n=3) and mutant lungs (n=3). All graphs show mean+s.e.m. ns, non-significant; *P≤0.05, **P≤0.01, ****P≤0.0001 (unpaired two-tailed t-test). Scale bars: 50 µm.

Mice

The following mice were used in this study: conditional *Pdgfa* knockout mice (*Pdgfa*$^{fl/fl}$) (*Pdgfa*^{tm1Vlcg}; Andrae et al., 2014), heterozygous global *Pdgfa* knockout mice (*Pdgfa*$^{+/-}$) (*Pdgfa*^{tm1Cbet}; Boström et al., 1996), *Pdgfra*^{GFP} reporter mice (*Pdgfra*$^{tm11(EGFP)Sor}$; Hamilton et al., 2003) constitutive *Spc-cre*-expressing mice (*Spc-cre*) [Tg(*Sftpc-cre*)^{tm1Blh}; Okubo and Hogan, 2004] and inducible *Spc-cre*-expressing mice (*Spc-cre*^{ERT2}) [*Sftpctm1*$^{(cre/ERT2)Blh}$; Rock et al., 2011]. *Pdgfa*$^{+/-}$ mice were first crossed with either *Spc-cre* or *Spc-cre*^{ERT2} to generate *Pdgfa*$^{+/-}$*; Spc-cre* and *Pdgfa*$^{+/-}$*; Spc-cre*^{ERT2} mice, which were further crossed with *Pdgfa*$^{fl/fl}$. Genotypes were confirmed by PCR using the primers described in Table S1.

Tamoxifen induction

Pups received five doses of tamoxifen [100 µl of 20 mg/ml solution (Sigma-Aldrich, H6278) administered to the lactating mother on consecutive days] and lungs were harvested at the desired time points after induction.

Lung tissue preparation

Mice were anesthetized with a cocktail of ketamine (75 mg/kg; Ketaminol® vet., Intervet AB, Sweden) and Dexdomitor (0.5 mg/kg; Orion Corporation, Finland) and perfused with PBS through the right ventricle of the heart, followed by perfusion with 4% formaldehyde (9713.5000, VWR). Lungs were inflated through the trachea with 4% formaldehyde and fixed at room temperature for 30 min (if X-gal staining was performed) or 4 h and washed in PBS at 4°C overnight. X-gal staining was performed as previously described (Gouveia et al., 2017). Lungs for cryosections were soaked in 30% sucrose and embedded in Neg-50 OCT (Richard Allan Scientific, 6502) whereas lungs for paraffin sections were dehydrated in a series of ethanol (70%, 95%, 99%) and xylene, followed by paraffin embedding. Lungs for vibratome sections were inflated with 2% low melting agarose, immersion fixed for 4 h in 4% formaldehyde at 4°C and washed in PBS overnight.

Lung histology

Paraffin sections (5 µm) were rehydrated in xylene and a series of ethanol (99%, 95%, 80%) for 4 min each. Sections were stained with Hematoxylin and Eosin and mounted in Neo-mount (109016, Merck). To calculate the MLI, bright-field images were obtained with a Zeiss Axioimager Microscope at 40× magnification. Eleven horizontal lines were superimposed on each image, and the intersections between the lines and the alveolar walls were counted. The number of lines was multiplied by the length of the lines and divided by the number of interception points. Thirty random images were taken from each lung and the MLI was manually calculated.

Immunostaining of lung tissue

Rehydrated paraffin sections (5 µm) were subjected to antigen retrieval for 20 min in a water bath at 95°C with Target Retrieval Solution, citrate pH 6.0 (Dako Cytomation, S2369). Sections were washed in dH_2O afterwards and then subjected to the same treatment as cryosections. Cryosections (20 µm) were washed in PBS and blocked overnight in 1% bovine serum albumin (BSA) and 0.5% Triton X-100 at 4°C. Sections were incubated at 4°C overnight with primary antibodies, washed with PBS and incubated for 1 h at room temperature with secondary antibodies. After washes in PBS, sections were mounted in Prolong Gold anti-fade reagent with DAPI (Invitrogen, P36931). Vibratome sections (100 µm) were blocked overnight in 1% BSA and 0.5% Triton X-100 at 4°C, incubated with primary antibodies for 48 h at 4°C, washed in PBS and incubated with secondary

Development (2018) 145, dev161976. doi:10.1242/dev.161976

antibodies overnight at 4°C. Sections were stained with Hoechst (1:10,000, Invitrogen, 33342) for 10 min and mounted in Prolong Gold anti-fade reagent (Invitrogen, P36930). Primary antibodies used were: mouse anti-human Asma (alpha-smooth muscle actin) conjugated to Cy3 (1:200, Sigma-Aldrich, C6198, Lot# 037M4783V), goat anti-SPC (1:100, Santa Cruz, sc7706, Lot# A2712), rabbit anti-Ki67 (1:100, Abcam, 15580, Lot# GR3184863-1), rabbit anti-cleaved caspase 3 (1:100, Cell Signaling Technologies, 9661, Lot# 45) and rabbit anti-ADFP (1:100, Thermo Fisher Scientific, PA1-16972, Lot# Sh2431603A). Secondary antibodies used were: Alexa Fluor 555-conjugated donkey anti-goat (1:200, Molecular Probes, Lot# 1697092); Alexa Fluor 647-conjugated donkey anti-rabbit (1:200, Molecular Probes, Lot# 1182665) and Alexa Fluor 568-conjugated donkey anti-rabbit (1:200, Molecular Probes, Lot# 1558655).

Imaging and image analysis

Confocal images were acquired using a TCS SP8 Laser Scanning Microscope (Leica) and images were processed using ImageJ software (NIH). Quantifications were performed using Imaris image analysis software (Bitplane, Oxford) with spots and surface modules. A total of ten images of 40× fields per lung were analyzed.

RNA isolation, cDNA synthesis and quantitative PCR

For gene expression analysis, whole left lung lobes were harvested and immersed in RNAlater (Qiagen). To extract RNA, the RNeasy Mini Kit (Qiagen) was used and cDNA was synthesized from 1 µg of total RNA using the iScript cDNA synthesis kit (Bio-Rad). Quantitative real-time PCR was performed using the CFX-96 Real Time System (Bio-Rad) and the following Taqman probes: *Pdgfa* (Mm00435540_m1, Thermo Fisher Scientific), *Pdgfra* (Mm00440701_m1, Thermo Fisher Scientific), *Kras* (Mm00517492_m1, Thermo Fisher Scientific) and *Hbegf* (Mm00439306_m1, Thermo Fisher Scientific). Each qPCR was replicated three times and sample results were normalized to 18 s rRNA endogenous control (X03201.1, Applied Biosystems). Fold change quantifications were performed using the Livak method ($2^{-\Delta\Delta Ct}$) (Schmittgen and Livak, 2008).

Statistical analysis

All quantification data assembly and statistical analyses were performed using GraphPad Prism version 6 for Mac (GraphPad Software). Student's *t*-test (unpaired and two tailed) was used to analyze significant differences between the means of two groups (control versus knockout). For each time point, all the analysis was performed with three different mice per group (three controls and three mutants). All results are presented as mean+s.e.m. $P<0.05$ was considered statistically significant.

Acknowledgements

We thank Jana Chmielniakova, Cecilia Olsson, Pia Peterson, Helene Leksell and Veronika Sundell for technical assistance with the mice. We also thank the BioVis core facility at Uppsala University for microscopy technical support.

Competing interests

The authors declare no competing or financial interests.

Author contributions

Conceptualization: C.B., J.A.; Methodology: L.G., C.B., J.A.; Validation: L.G., C.B., J.A.; Formal analysis: L.G.; Investigation: L.G.; Resources: C.B.; Writing - original draft: L.G.; Writing - review & editing: L.G., C.B., J.A.; Visualization: L.G.; Supervision: C.B., J.A.; Project administration: J.A.; Funding acquisition: C.B., J.A.

Funding

This study was supported by research grants from AstraZeneca AB through the Integrated Cardio Metabolic Centre (to C.B.), the Swedish Research Council (Vetenskapsrådet; 2015-00550 to C.B.), the European Research Council (AdG294556 to C.B.), the Fondation Leducq (14CVD02 to C.B.), Swedish Cancer Society (Cancerfonden; 150735 to C.B.), Knut och Alice Wallenbergs Stiftelse (2015.0030 to C.B.), Magnus Bergvalls Stiftelse (2014-00174 to J.A.) and Åke Wiberg Stiftelse (362565719, 946216308 to J.A.).

Supplementary information

Supplementary information available online at
http://dev.biologists.org/lookup/doi/10.1242/dev.161976.supplemental

References

Andrae, J., Gallini, R. and Betsholtz, C. (2008). Role of platelet-derived growth factors in physiology and medicine. *Genes Dev.* **22**, 1276-1312.

Andrae, J., Ehrencrona, H., Gallini, R., Lal, M., Ding, H. and Betsholtz, C. (2013). Analysis of mice lacking the heparin-binding splice isoform of platelet-derived growth factor A. *Mol. Cell. Biol.* **33**, 4030-4040.

Andrae, J., Gouveia, L., He, L. and Betsholtz, C. (2014). Characterization of platelet-derived growth factor-a expression in mouse tissues using a lacZ knock-in approach. *PLoS ONE* **9**, e105477.

Andrae, J., Gouveia, L., Gallini, R., He, L., Fredriksson, L., Nilsson, I., Johansson, B. R., Eriksson, U. and Betsholtz, C. (2016). A role for PDGF-C/PDGFRα signaling in the formation of the meningeal basement membranes surrounding the cerebral cortex. *Biol. Open* **5**, 461-474.

Barkauskas, C. E., Cronce, M. J., Rackley, C. R., Bowie, E. J., Keene, D. R., Stripp, B. R., Randell, S. H., Noble, P. W. and Hogan, B. L. M. (2013). Type 2 alveolar cells are stem cells in adult lung. *J. Clin. Invest.* **123**, 3025-3036.

Barron, L., Gharib, S. A. and Duffield, J. S. (2016). Lung pericytes and resident fibroblasts. *Am. J. Pathol.* **186**, 2519-2531.

Beers, M. F. and Morrisey, E. E. (2011). The three R's of lung health and disease: repair, remodeling, and regeneration. *J. Clin. Invest.* **121**, 2065-2073.

Boström, H., Willetts, K., Pekny, M., Levéen, P., Lindahl, P., Hedstrand, H., Pekna, M., Hellström, M., Gebre-Medhin, S., Schalling, M. et al. (1996). PDGF-A signaling is a critical event in lung alveolar myofibroblast development and alveogenesis. *Cell* **85**, 863-873.

Boström, H., Gritli-Linde, A. and Betsholtz, C. (2002). PDGF-A/PDGF alpha-receptor signaling is required for lung growth and the formation of alveoli but not for early lung branching morphogenesis. *Dev. Dyn.* **223**, 155-162.

Branchfield, K., Li, R., Lungova, V., Verheyden, J. M., McCulley, D. and Sun, X. (2016). A three-dimensional study of alveologenesis in mouse lung. *Dev. Biol.* **409**, 429-441.

Chapman, H. A. (2011). Epithelial-mesenchymal interactions in pulmonary fibrosis. *Annu. Rev. Physiol.* **73**, 413-435.

Desai, T. J., Brownfield, D. G. and Krasnow, M. A. (2014). Alveolar progenitor and stem cells in lung development, renewal and cancer. *Nature* **507**, 190-194.

Endale, M., Ahlfeld, S., Bao, E., Chen, X., Green, J., Bess, Z., Weirauch, M. T., Xu, Y. and Perl, A.-K. (2017). Temporal, spatial, and phenotypical changes of PDGFRα expressing fibroblasts during late lung development. *Dev. Biol.* **425**, 161-175.

Fruttiger, M., Karlsson, L., Hall, A. C., Abramsson, A., Calver, A. R., Boström, H., Willetts, K., Bertold, C. H., Heath, J. K., Betsholtz, C. et al. (1999). Defective oligodendrocyte development and severe hypomyelination in PDGF-A knockout mice. *Development* **126**, 457-467.

Gnessi, L., Basciani, S., Mariani, S., Arizzi, M., Spera, G., Wang, C., Bondjers, C., Karlsson, L. and Betsholtz, C. (2000). Leydig cell loss and spermatogenic arrest in platelet-derived growth factor (PDGF)-A-deficient mice. *J. Cell Biol.* **149**, 1019-1026.

Gouveia, L., Betsholtz, C. and Andrae, J. (2017). Expression analysis of platelet-derived growth factor receptor alpha and its ligands in the developing mouse lung. *Physiol. Rep.* **5**, e13092.

Green, J., Endale, M., Auer, H. and Perl, A.-K. T. (2016). Diversity of interstitial lung fibroblasts is regulated by platelet-derived growth factor receptor α kinase activity. *Am. J. Respir. Cell Mol. Biol.* **54**, 532-545.

Hamilton, T. G., Klinghoffer, R. A., Corrin, P. D. and Soriano, P. (2003). Evolutionary divergence of platelet-derived growth factor alpha receptor signaling mechanisms. *Mol. Cell. Biol.* **23**, 4013-4025.

Karlsson, L., Bondjers, C. and Betsholtz, C. (1999). Roles for PDGF-A and sonic hedgehog in development of mesenchymal components of the hair follicle. *Development* **126**, 2611-2621.

Karlsson, L., Lindahl, P., Heath, J. K. and Betsholtz, C. (2000). Abnormal gastrointestinal development in PDGF-A and PDGFR-(alpha) deficient mice implicates a novel mesenchymal structure with putative instructive properties in villus morphogenesis. *Development* **127**, 3457-3466.

Lindahl, P., Karlsson, L., Hellström, M., Gebre-Medhin, S., Willetts, K., Heath, J. K. and Betsholtz, C. (1997). Alveogenesis failure in PDGF-A-deficient mice is coupled to lack of distal spreading of alveolar smooth muscle cell progenitors during lung development. *Development* **124**, 3943-3953.

McGowan, S. E. (2014). Paracrine cellular and extracellular matrix interactions with mesenchymal progenitors during pulmonary alveolar septation. *Birth Defects Res. Part A Clin. Mol. Teratol.* **100**, 227-239.

McGowan, S. (2017). Understanding the developmental pathways pulmonary fibroblasts may follow during alveolar regeneration. *Cell Tissue Res.* **367**, 707-719.

McGowan, S. E. and McCoy, D. M. (2017). Platelet-derived growth factor receptor-alpha (PDGFRα) and Ras-related C3 botulinum toxin substrate-1 (Rac1) regulate mechano-responsiveness of lung fibroblasts. *AJP: Lung Cell. Mol. Physiol.* **313**, L1174-L1187.

Moiseenko, A., Kheirollahi, V., Chao, C.-M., Ahmadvand, N., Quantius, J., Wilhelm, J., Herold, S., Ahlbrecht, K., Morty, R. E., Rizvanov, A. A. et al. (2017). Origin and characterization of alpha smooth muscle actin-positive cells during murine lung development. *Stem Cells* **35**, 1566-1578.

Morrisey, E. E. and Hogan, B. L. M. (2010). Preparing for the first breath: genetic and cellular mechanisms in lung development. *Dev. Cell* **18**, 8-23.
Ntokou, A., Klein, F., Dontireddy, D., Becker, S., Bellusci, S., Richardson, W. D., Szibor, M., Braun, T., Morty, R. E., Seeger, W. et al. (2015). Characterization of the platelet-derived growth factor receptor-α-positive cell lineage during murine late lung development. *Am. J. Physiol. Lung Cell Mol. Physiol.* **309**, L942-L958.
Okubo, T. and Hogan, B. L. M. (2004). Hyperactive Wnt signaling changes the developmental potential of embryonic lung endoderm. *J. Biol.* **3**, 11.
Pinkerton, K., Harding, R. and Plopper, C. (2014). *The Lung: Development, Aging and the Environment*, 2nd edn. London: Elsevier Academic Press.
Popova, A. P. (2013). Mechanisms of bronchopulmonary dysplasia. *J. Cell Commun. Signal.* **7**, 119-127.
Popova, A. P., Bentley, J. K., Cui, T. X., Richardson, M. N., Linn, M. J., Lei, J., Chen, Q., Goldsmith, A. M., Pryhuber, G. S. and Hershenson, M. B. (2014). Reduced platelet-derived growth factor receptor expression is a primary feature of human bronchopulmonary dysplasia. *AJP: Lung Cell. Mol. Physiol.* **307**, L231-L239.
Roan, E. and Waters, C. M. (2011). What do we know about mechanical strain in lung alveoli? *AJP: Lung Cell. Mol. Physiol.* **301**, L625-L635.
Rock, J. R., Barkauskas, C. E., Cronce, M. J., Xue, Y., Harris, J. R., Liang, J., Noble, P. W. and Hogan, B. L. M. (2011). Multiple stromal populations contribute to pulmonary fibrosis without evidence for epithelial to mesenchymal transition. *Proc. Natl. Acad. Sci. USA* **108**, E1475-E1483.
Schmittgen, T. D. and Livak, K. J. (2008). Analyzing real-time PCR data by the comparative C(T) method. *Nat. Protoc.* **3**, 1101-1108.
Shi, W., Bellusci, S. and Warburton, D. (2007). Lung development and adult lung diseases. *Chest* **132**, 651-656.
Soriano, P. (1997). The PDGF alpha receptor is required for neural crest cell development and for normal patterning of the somites. *Development* **124**, 2691-2700.
Tamada, M., Perez, T. D., Nelson, W. J. and Sheetz, M. P. (2007). Two distinct modes of myosin assembly and dynamics during epithelial wound closure. *J. Cell Biol.* **176**, 27-33.
Treutlein, B., Brownfield, D. G., Wu, A. R., Neff, N. F., Mantalas, G. L., Espinoza, F. H., Desai, T. J., Krasnow, M. A. and Quake, S. R. (2014). Reconstructing lineage hierarchies of the distal lung epithelium using single-cell RNA-seq. *Nature* **509**, 371-375.
Tsao, P.-N., Matsuoka, C., Wei, S.-C., Sato, A., Sato, S., Hasegawa, K., Chen, H.-K., Ling, T.-Y., Mori, M., Cardoso, W. V. et al. (2016). Epithelial Notch signaling regulates lung alveolar morphogenesis and airway epithelial integrity. *Proc. Natl. Acad. Sci. USA* **113**, 8242-8247.
Vedula, S. R. K., Peyret, G., Cheddadi, I., Chen, T., Brugués, A., Hirata, H., Lopez-Menendez, H., Toyama, Y., de Almeida, L. N., Trepat, X. et al. (2015). Mechanics of epithelial closure over non-adherent environments. *Nat. Commun.* **6**, 6111.
Warburton, D., El-Hashash, A., Carraro, G., Tiozzo, C., Sala, F., Rogers, O., Langhe, S. D., Kemp, P. J., Riccardi, D., Torday, J. et al. (2010). Lung organogenesis. In *Organogenesis in Development* (ed. P. Koopman), pp. 73-158. London: Elsevier.
Zepp, J. A., Zacharias, W. J., Frank, D. B., Cavanaugh, C. A., Zhou, S., Morley, M. P. and Morrisey, E. E. (2017). Distinct mesenchymal lineages and niches promote epithelial self-renewal and myofibrogenesis in the lung. *Cell* **170**, 1134-1148.e10.